Supporting Information for MnB_2 nanosheet and nanotube: stability, electronic structures, novel functionalization and application for Li-ion battery.

Bingwen Zhang,[1,2†] Lele Fan,[3†] Jingsan Hu,[2] Jianfei Gu,[2] Baolin Wang,[3] and Qinfang Zhang[*1]
[1] *School of materials science and engineering, Yancheng Institute of Technology, Yancheng 224051, China.*
[2] *National Laboratory of Solid State Microstructures and Department of Physics, Nanjing University, Nanjing 210093, China.*
[3] *Laboratory for Advanced Technology in Environmental Protection of Jiangsu Province, Yancheng Institute of Technology, Yancheng, 224051, China.*
[†] *These authors contributed equally to this work. and*
[*] *E-mail: qfangzhang@gmail.com.*

This Supporting Information includes the cleavage energy of monolayer MnB_2 from bulk MnB_2, *Ab initio molecular dynamics* (AIMD) results of h-MnB_2 and t-MnB_2 with O_2 molecules adsorption, the magnetic property of bilayer MnB_2 nanosheets, the magnetic property of bulk MnB_2, the crystal field splitting of h-MnB_2 nanosheet, the electronic band of passivated h-MnB_2 by halogen, the AIMD results of (10_0) zigzag h-MnB_2 nanosheet at 400 K and 500 K, the band structure and density of states of (10_0) zigzag h-MnB_2 nanosheet and the bending property of TmB_2 nanosheets.

I. CLEAVAGE ENERGY OF MONOLAYER MNB_2 FROM BULK MNB_2

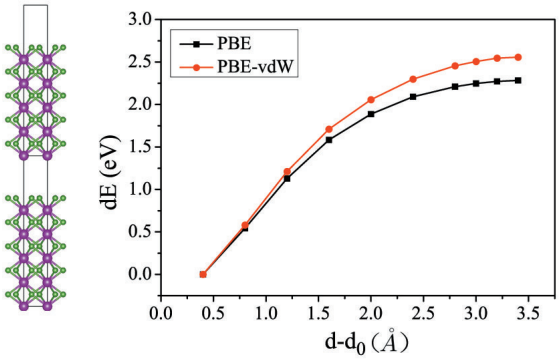

FIG. S1. The relative energy as function of cleavage distance $(d - d_0)$ from bulk MnB_2.

II. AIMD RESULTS OF H-MNB_2 AND T-MNB_2 WITH O_2 MOLECULES ADSORPTION

We performed the AIMD calculations at 300 K for the condition of O_2 molecules adsorption, The result shows that the bond between Mn-B, B-B and O-O are obviously twisted, which suggests that the MnB_2 nanosheets is not suitable to be exposed to air.

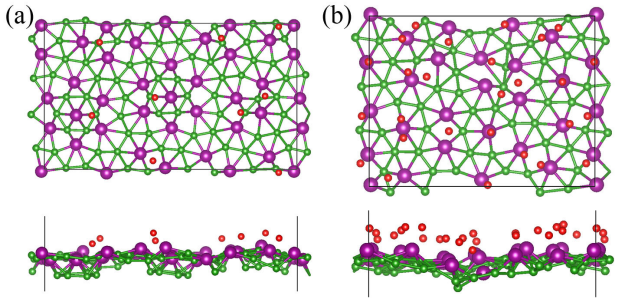

FIG. S2. The geometric structures of h-MnB_2 (a) and t-MnB_2 (b) nanosheet after the AIMD calculations at 300 K.

III. MAGNETIC PROPERTY OF BILAYER MNB_2 NANOSHEETS

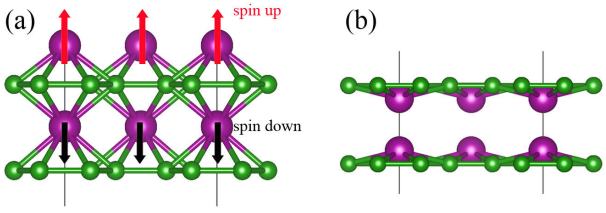

FIG. S3. The magnetic property of bilayer nanosheets of h-MnB_2 (a) and t-MnB_2 (b).

IV. MAGNETIC PROPERTY OF BULK MNB_2

The FM, AAFM, and CAFM states of bulk MnB_2 are shown in Fig. S4, the AAFM state is the ground state, the FM state is 0.73 eV higher than the AAFM, and the CAFM state is 1.69 eV than the AAFM state. The Monte Carlo result is shown in FiG. S5, the result shows that the Néel temperature is about 740 K.

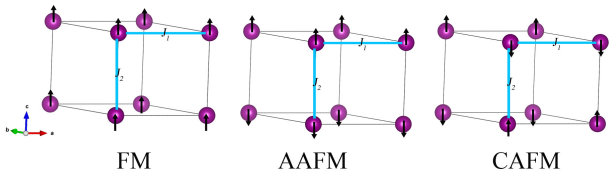

FIG. S4. Three different magnetic states of bulk MnB_2.

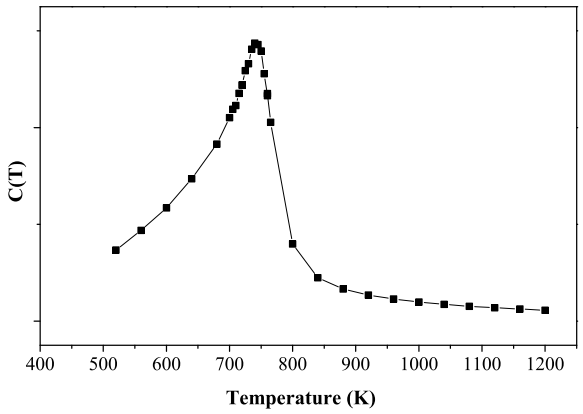

FIG. S5. Specific heat as a function of temperature.

V. CRYSTAL FIELD SPLITTING OF H-MNB_2 NANOSHEET

The h-MnB_2 nanosheet is in C_{6v} symmetry, each Mn atom has six ligands of B atoms. The d orbitals wave functions can be expanded in terms of spherical harmonics:

$$\begin{cases} d_{xz} = \frac{\sqrt{2}}{2}(Y_{21} + Y_{2-1}) = \sqrt{\frac{15}{4\pi}}\frac{xz}{r^2} \\ d_{yz} = \frac{\sqrt{2}}{2i}(Y_{21} - Y_{2-1}) = \sqrt{\frac{15}{4\pi}}\frac{yz}{r^2} \\ d_{xy} = \frac{\sqrt{2}}{2i}(Y_{22} - Y_{2-2}) = \sqrt{\frac{15}{2\pi}}\frac{xy}{r^2} \\ d_{x^2-y^2} = \frac{\sqrt{2}}{2}(Y_{22} + Y_{2-2}) = \sqrt{\frac{15}{16\pi}}\frac{x^2-y^2}{r^2} \\ d_{z^2} = Y_{20} = \sqrt{\frac{5}{16\pi}}\frac{2z^2-x^2-y^2}{r^2} \end{cases} \tag{1}$$

Here x, y and z are the three components of $\vec{r}$(x,y,z), which is position vector of d electrons. With in the electrostatic crystal field approximation, the ligands could be treated as point charges perturbing the fivefold degenerate d electron energy level, crystal splitting could be evaluated from crystal electric potential:

$$V(r) = \sum_i^6 \frac{q_i}{|\vec{R_i} - \vec{r}|} \tag{2}$$

We take the approximation of expanding the crystal electric potential without considering the terms higher than six order, and then integrating over crystal electric potential using the crystal wave functions above, the energy level of

the five orbitals are:

$$\begin{cases} E_{d_{Z^2}} & = \frac{3<r^2>(45<r^2>-11a^2)}{14a^4} \\ E_{d_{x^2-y^2}} & = \frac{3(85<r^4>-6a^2<r^2>)}{28a^4} \\ E_{d_{xy}} & = \frac{3(85<r^4>-6a^2<r^2>)}{28a^4} \\ E_{d_{xz}} & = \frac{3<r^2>(40<r^2>-9a^2)}{14a^4} \\ E_{d_{yz}} & = \frac{3<r^2>(40<r^2>-9a^2)}{14a^4} \end{cases} \tag{3}$$

Here, a is the bond length of Mn and B, the results show that the d orbitals splits to three group, singlet d_{z^2}, double degenerate d_{xy} and $d_{x^2-y^2}$ as well as double degenerate d_{xz} and d_{yz}.

VI. THE ELECTRONIC BAND STRUCTURES OF F/CL PASSIVATED H-MNB$_2$ NANOSHEET WITH DIFFERENT STRAINS

We plotted the band structures of F or Cl passivated h-MnB_2 nanosheet. The discrepancy of h-MnB_2Cl band structures under different tensile strains is tiny while the dispersion of bands under the strain of -4% are cross the Fermi energy at Γ point, which is obviously changed.

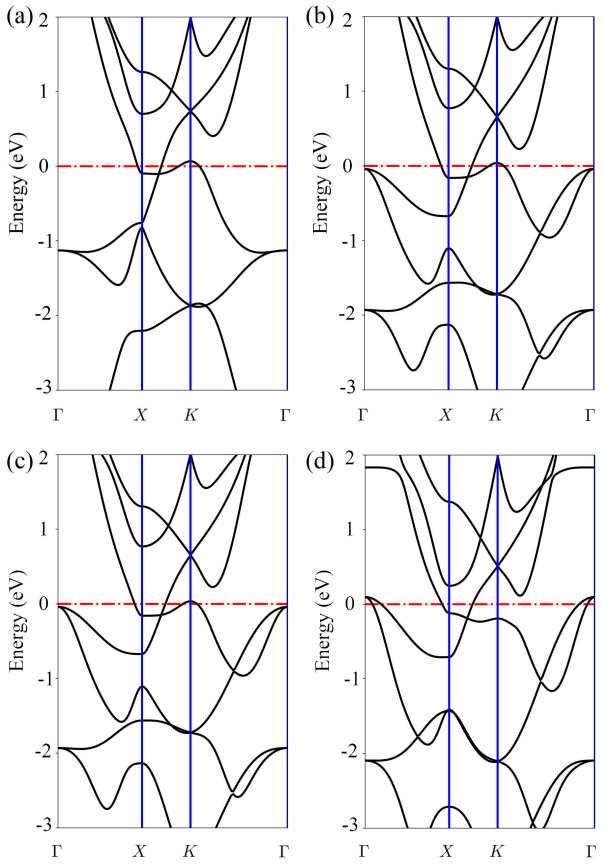

FIG. S6. Band structures: (a) h-MnB_2F with strain of $e = 2\%$; (b), (c) and (d) are h-MnB_2Cl in strain of $e = 2\%, e = 0\%$ and $e = -4\%$, respectively.

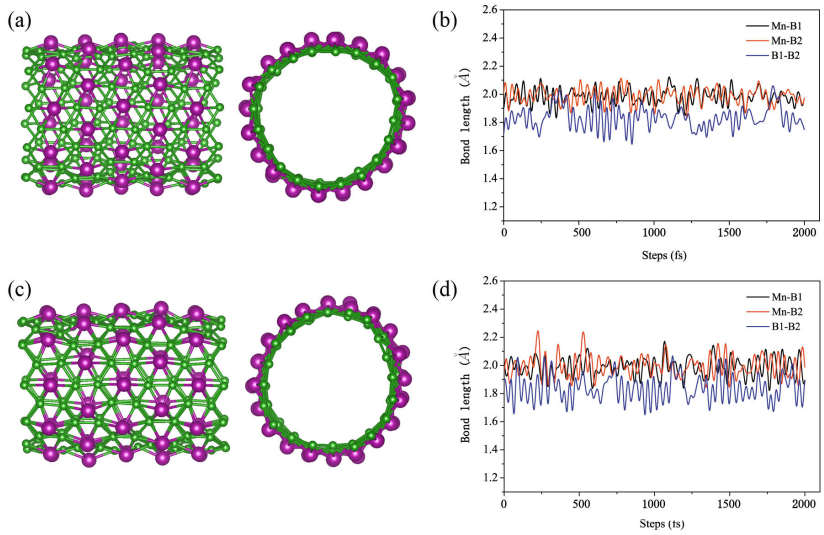

FIG. S7. The AIMD result of (10_0) zigzag h-MnB_2 nanotube at 400 K(a+b) and 500 K(c+d).

VII. THE AIMD RESULTS AND ELECTRONIC BAND STRUCTURE AND DENSITY OF SATES OF (10_0) ZIGZAG H-MNB_2 NANOTUBE

It reveals that the (10_0) zigzag h-MnB_2 nanotube is metallic from the band structure and the density of states of Fig. S8, which is beneficial for electron transport.

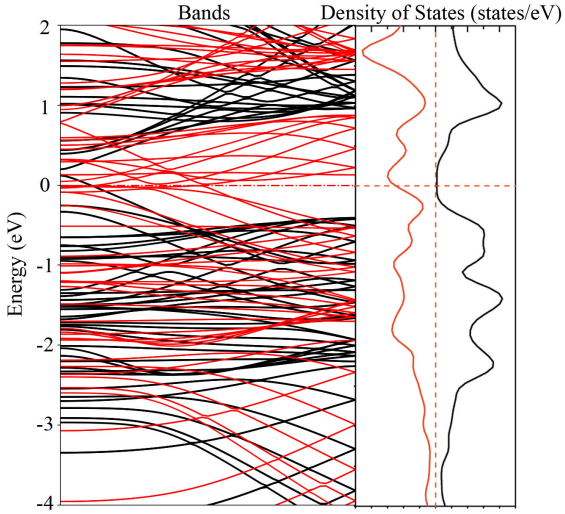

FIG. S8. Band structure and density of sates of (10_0) zigzag h-MnB_2 nanotube.

VIII. BENDING PROPERTY OF TMB_2 IN C_{6v} POINT GROUP

We adopted a simple nanobibbon method to confirm the bending property of different TmB_2 nanosheets, which are in C_{6v} point group.

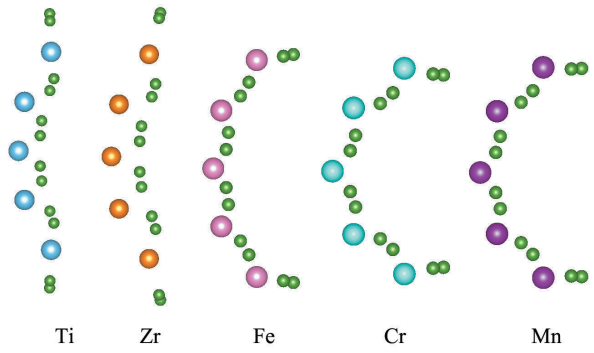

FIG. S9. Bending property of TmB_2 nanosheets.